Chang *et al. Chem. Biol. Technol. Agric.* (2024) 11:64
https://doi.org/10.1186/s40538-024-00587-9

Chemical and Biological Technologies in Agriculture

RESEARCH

Open Access

The isolation, structure characterizations and anti-photoaging activities of sulfated polysaccharides isolated from *Sargassum fusiforme*

Shiyuan Chang[1,2], Yifan Chen[1,2], Huamai Qiu[1,2], Biyang Zhu[1,2], Lijun You[1,2*] and Peter Chi Keung Cheung[3]

Abstract

Background Our previous study found that crude polysaccharide extracted from *Sargassum fusiforme* (PSF) exhibited excellent anti-photoaging activity, but the composition responsible for this activity remained unknown.

Results In this study, three fractions (P1, P2 and P3) obtained by hot water extraction and column chromatographic separation from PSF were structurally characterized. The anti-photoaging activities of these isolated polysaccharides were evaluated using HaCaT cells. The results showed that P1, P2 and P3 were acidic polysaccharides with 42.94%, 40.75% and 2.21% uronic acid. In addition, the contents of sulfate groups were 3.01%, 10.05% and 7.44%, respectively. Moreover, their content of reducing sugar was low, and none of the fractions had a triple-stranded helical structure. P1 had the largest average molecular weight of 208.89 kDa, while P2 and P3 had a relatively lower molecular weight of 154.09 and 151.71 kDa, respectively. Treatment with P2 effectively safeguarded the viability of HaCaT cells exposed to UVB irradiation. Additionally, it inhibited the secretion of MMP-1 and MMP-3 while elevating the content of hydroxyproline (HYP) in the cell supernatant. Methylation and NMR analysis suggested the main structure of P2 might be →[4)-β-ManA-(1]$_{23}$→4)-β-ManA-(1→3)-β-D-Glc*p*-(1→4)-β-D-Glc*p*-(1→4)-β-D-Glc*p*-(1→. The two terminal groups of β-ManA-(1→and β-D-Glc*p*-(1→were connected via the glycosidic bonds of →3, 4)-*O*-3 in β-ManA-(1→and O-6 in →4, 6)-β-D-Glc*p*-(1→, respectively.

Conclusions These findings will open new avenues for exploring the potential use of *Sargassum fusiforme* polysaccharide, particularly P2, as a functional ingredient with anti-photoaging activity.

Keywords *Sargassum fusiforme*, Polysaccharide, Anti-photoaging, Alginate

*Correspondence:
Lijun You
feyoulijun@scut.edu.cn
Full list of author information is available at the end of the article

© The Author(s) 2024. **Open Access** This article is licensed under a Creative Commons Attribution 4.0 International License, which permits use, sharing, adaptation, distribution and reproduction in any medium or format, as long as you give appropriate credit to the original author(s) and the source, provide a link to the Creative Commons licence, and indicate if changes were made. The images or other third party material in this article are included in the article's Creative Commons licence, unless indicated otherwise in a credit line to the material. If material is not included in the article's Creative Commons licence and your intended use is not permitted by statutory regulation or exceeds the permitted use, you will need to obtain permission directly from the copyright holder. To view a copy of this licence, visit http://creativecommons.org/licenses/by/4.0/. The Creative Commons Public Domain Dedication waiver (http://creativecommons.org/publicdomain/zero/1.0/) applies to the data made available in this article, unless otherwise stated in a credit line to the data.

Graphical Abstract

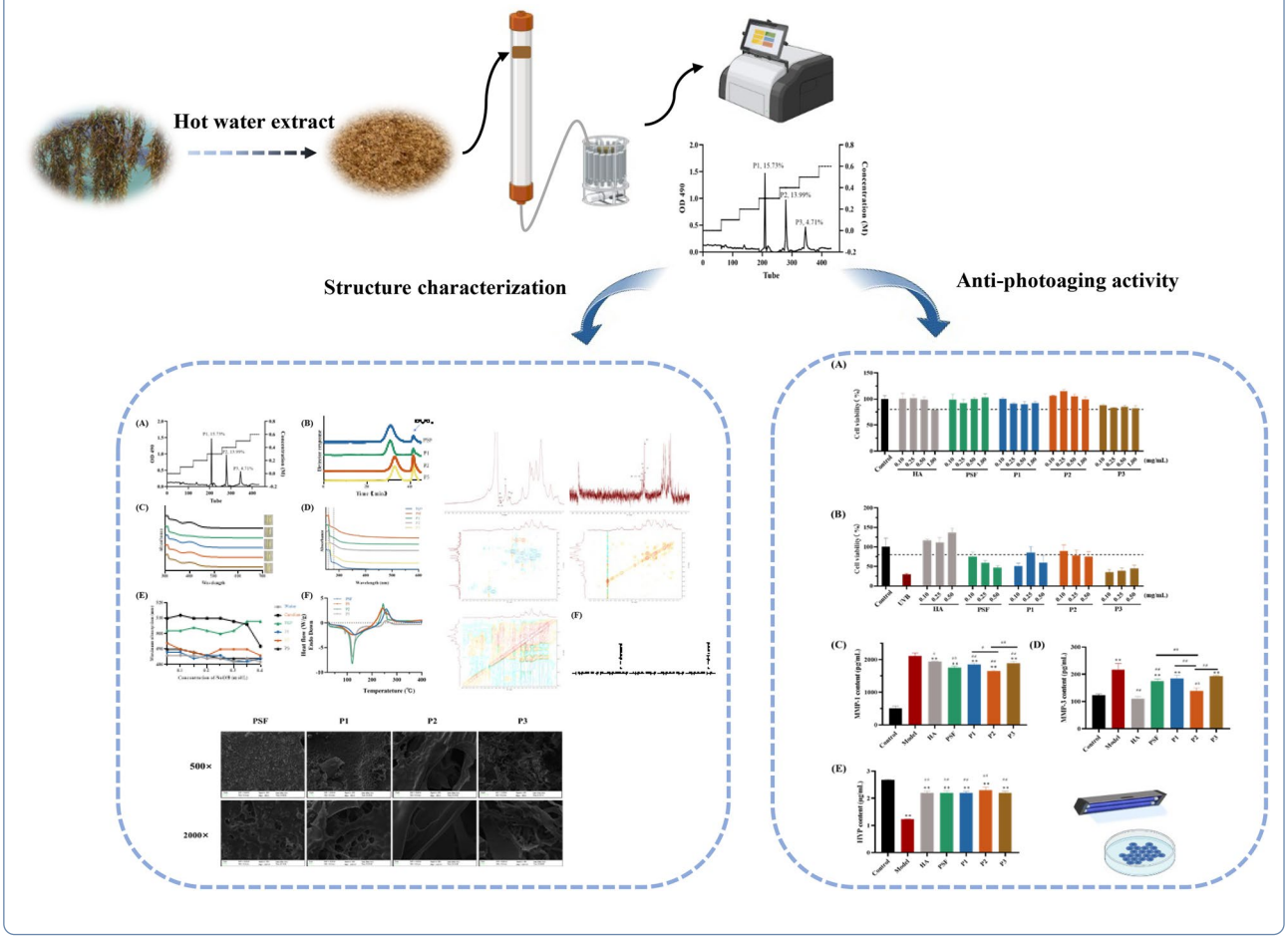

Introduction

Marine algae are abundant and valuable resources in the ocean, which have traditionally been used for food, fertilizer, and therapeutic purposes for a long time [1]. They are mainly classified into three main groups: red algae (Rhodophyta), green algae (Chlorophyta) and brown algae (Phaeophyta) based on their thallus color [2]. The global seaweed market is estimated to reach $30.2 billion by 2028, at a compound annual growth rate (CAGR) of 12.6% [3]. As the leading producer globally, China accounts for 27% of the world's annual harvest of wild seaweeds and 72% of the world's annual crop of cultivated seaweeds [4]. However, only a small amount of seaweed is consumed or simple processing. The majority of the seaweed resources have been underutilized, resulting in a significant waste problem [5].

More recently, marine algae and their extracts have been utilized as a novel source of biological raw materials for functional ingredients [6]. *Sargassum fusiforme*, a typical brown algae, is widely distributed in China, Japan, South Korea, and North Korea. It is also known as jade grass, antler tip, and "longevity dish" [7]. Previous studies have suggested that *Sargassum fusiforme* possesses various bioactivities such as antioxidant capacity [8], anticancer effects [9], anti-inflammatory properties [10, 11], and skin protection [12]. Besides, polysaccharides were regarded as one of the vital compounds that contribute to its bioactivities [7]. Plant polysaccharides have complex molecular structures with varying degrees and lengths of branching [13]. The polysaccharide from *Sargassum fusiforme* is mainly composed of alginates, laminarans and fucoidans. Different purification processes and raw materials lead to the diversity of their composition and pharmacological activities [7]. Our previous studies found that crude polysaccharides from *Sargassum fusiforme* possessed potential anti-photoaging activity [12, 14]. However, the main structural characteristics responsible for anti-photoaging activity are unknown. This work

aims to move the research further into detailed structural descriptions of polysaccharide from *Sargassum fusiforme* with anti-photoaging activity.

In the present study, polysaccharides were extracted from *Sargassum fusiforme* by hot water extraction and then isolated by DEAE Sepharose Fast Flow chromatographic column. The structural characteristics and anti-photoaging activities of the isolated polysaccharides were investigated. Moreover, the precise structure of the isolated fractions with the best anti-photoaging activity was determined. The study may provide the scientific basis for further development and utilization of *Sargassum fusiforme* as a food ingredient or pharmaceutical additive.

Materials and methods

Materials

Sargassum fusiform was collected in May 2019 in Dongtou District, Wenzhou, Zhejiang, China, and authenticated by Collagen of Science, Shantou University. DEAE Sepharose Fast Flow was provided by GE (Fairfield, Connecticut, USA). Monosaccharide standards (Glucose, Fucose, Rhamnose, Arabinose, Galactose, Xylose, Mannose, Galacturonic acid, Guluronic acid, Glucuronic acid, Mannuronic acid) and dextran standards of different molecular weights (MW) were obtained from Sigma–Aldrich (St Louis, MO, USA). Hyaluronic acid (HA, 97%) was supplied from Shanghai Maclean Biochemical Co. (Shanghai, China). Human immortalized keratinocytes (HaCaT) cell was purchased from the Cell Resource Center, Shanghai Institute of Biological Sciences (Shanghai, China). Dulbecco's modified eagle's medium (DMEM) was provided by Gibco Co. (Grand Island, New York, USA). Methyl thiazolyl tetrazolium (MTT) and hydroxyproline (HYP) kits were purchased from Nanjing Jiancheng Institute of Biological Engineering Co. (Nanjing, Jiangsu, China). Matrix metallopeptidase 1 (MMP-1) ELISA kit was purchased from Neobioscience Technology Co. (Shenzhen, Guangdong, China). Matrix metallopeptidase 3 (MMP-3) ELISA kit was acquired from Multi Sciences (Lianke) Biotech Co., Ltd. (Hangzhou, Zhejiang, China).

Preparation and purification of polysaccharides from *Sargassum fusiform*

Polysaccharide of *Sargassum fusiform* (PSF) was prepared according to our previously reported method [15]. Briefly, PSF was prepared by hot water extraction (1:50, *m*/*v*) and 80% ethanol precipitation, followed by full ethanol removal and lyophilization. PSF (20 mg) was then dissolved in distilled water (10 mL) and loaded onto a DEAE Sepharose Fast Flow column (26 cm × 40 cm i.d.), then sequentially eluted with distilled water and different concentrations of NaCl solution (0.1, 0.2, 0.3, 0.4, 0.5, 1 M) in phosphate buffer solution with a flow rate of 1.0 mL/min. The elution fractions were collected in tubes every 10 mL and the polysaccharide content was determined by the phenol–sulfuric acid method at 490 nm by spectrophotometer (752 N, Shanghai Precision and Scientific Instrument Co., Ltd, Shanghai, China) [16]. The eluents from the same peak were merged, concentrated, and lyophilized (Martin Christ Lyophilizer, Alpha 1–2LDPlus, Osterodeam Harz, Germany).

Physicochemical and structural characterization

Molecular weight distribution

The molecular weight distribution was performed following the previously reported method [17]. Briefly, High-performance gel permeation chromatography (HPGPC) was equipped by an HPLC system (Waters, USA) with TSK-GEL G-6000 PWXL column (7.8 mm × 300 mm i.d., 13 μm, Tosoh Co, Tokyo, Japan), a TSK-GRL 3000 PWXL column (7.8 mm × 300 mm i.d., 7 μm, Tosoh Co, Tokyo, Japan) and a RID-10A refractive index detector (Waters, USA). Samples solution were filtered through a 0.22 μm Millipore filter and injected into HPLC. The column temperature was maintained at 35 °C and eluted with 0.02 M KH_2PO_4 solution at a flow rate of 0.5 mL/min.

Chemical composition

The content of protein was analyzed by the method of Coomassie Brilliant Blue using bovine serum albumin (BSA) as the standard [18]. The total phenol content was determined by the forintol colorimetric method, and gallic acid was used as a standard [19]. The contents of total sugar (using fucose as the standard) and reducing sugar (using glucose as the standard) were determined using the method of phenol sulfuric acid method and the 3, 5-dinitro salicylic acid (DNS) method, respectively [20, 21]. The contents of sulfate and uronic acid (using mannuronic acid as the standard) were determined according to the barium sulfate turbidimetric method [22] and m-hydroxyl diphenyl assay method [23], respectively.

Detection of I_2-KI

The sample solution (2 mL) was mixed with 1.2 mL of I_2-KI (containing 0.02% I_2 and 0.2% KI solution) for 30 min. Then the color change of the mixed solution was recorded and its UV–Vis spectrum (Shanghai Precision and Scientific Instrument Co., Ltd, Shanghai, China) was measured in the range of 250–700 nm with a wavelength interval of 2 nm [24]. Distilled water was used as the control.

Fourier transform infrared spectroscopy (FT-IR)

The FT-IR spectra were produced by a Bruker-Tensor 27 (Bruker Co. Ltd., Bergisch Gladbach, Germany). The

spectra were recorded from 4000 to 400 cm^{-1} at a resolution of 4 cm^{-1} and a scan count of 64. Dried polysaccharide (1 mg) powder was ground with KBr evenly and pressed to a thin pallet.

Monosaccharide composition

Samples (10 mg) were hydrolyzed with 4 M trifluoroacetic acid at 105 ℃ for 6 h, followed by rotary evaporation (Shanghai Yarong Biochemical Instrument Factory, Shanghai, China) to remove the residual trifluoroacetic acid. The sample was adjusted to a volume of 10 mL with ultrapure water and filtered through a 0.22 μm filter. The analysis of monosaccharide composition was performed using a Dionex™ CarboPac™ PA10 IC chromatography column (4 mm × 250 mm, 10 μm). The solution of NaOH (0.1 M) and NaAc (0.2 M) was used as mobile phases with a column temperature of 30 °C and a flow rate of 0.5 mL/min. Fucose, the most abundant neutral sugar found in *Sargassum fusiform*, was used as a standard. The identification and quantification of the different sugars were achieved by the retention time and peak area of monosaccharide standards.

Surface morphology observation

The surface morphology and microstructure of the samples were characterized using SEM (EVO 18, Carl Zeiss AG, Oberkohen, Baden-Wurttemberg, Germany) at 500× and 2000× magnification. After sputtering with a thin layer of gold, the lyophilized samples were observed under a vacuum at a 10.0 kV accelerating voltage.

Helical structure test

The polysaccharide with a helix structure could form complexes with Congo red ($C_{32}H_{22}N_6O_5S_2Na_3$), and its maximum absorption wavelength could be affected by NaOH. Polysaccharide solutions (2.5 mg/mL, 2 mL) were mixed with Congo red (100 μL, 80 mmol/L), and the transition from triple helix structure to single chain conformation of polysaccharide was observed by scanning the λmax of Congo red and polysaccharide with NaOH concentration ranging from 0 to 0.4 mol/L. The UV–Vis absorption spectrum was recorded on a 752 spectrophotometer (Shanghai Precision and Scientific Instrument Co., Ltd, Shanghai, China) in the range of 400–800 nm, with a wavelength interval of 2 nm [25]. The mixture solution of water and Congo red was used as the control.

Thermal properties

The thermal properties of PSF and isolated fractions were analyzed using a differential scanning calorimeter (DSC 250, TA Instruments, New Castle, DE, USA). Sealed aluminum plates containing samples were heated from 20 to 400 °C at a rate of 20 °C/min with a nitrogen flow rate of 50 mL/min.

Anti-photoaging activity in vitro of polysaccharides

The cytotoxicity of PSF and isolated fractions

Cells were cultured in DMEM supplemented with 10% fetal bovine serum and 1% penicillin/streptomycin and incubated at 37 ℃ in a 5% CO_2 atmosphere. HaCaT cells were cultured in 96-well plates at a density of 1×10^4 cells/well. After incubation for 24 h, the cells were treated with or without polysaccharides (dissolved in medium) for another 24 h. Afterward, the MTT (10 μL, 5 mg/mL) was added to each well and incubated for an additional 4 h. The culture medium was removed and then formazan was dissolved in dimethyl sulfoxide. The optical density was measured at 490 nm by spectrophotometer (SpectraMax 190, Molecular Devices, Sunnyvale, CA, USA). Cell viability was calculated as follows:

$$\text{Cell viability}(\%) = \frac{A1 - A0}{A2 - A0} \times 100 \quad (1)$$

where A1, A0, and A2 were the absorbances of the sample, blank, and control, respectively. The blank group represents wells containing medium without cells.

Effects of PSF and isolated fractions on the cell viability of photoaged HaCaT cells

The cell viability protective effects of polysaccharides on UVB-irradiated (HOPE–MED 814, Tianjin Hepu Company, Tianjin, China) HaCaT cells were performed similarly with the above cytotoxic assay. Briefly, the cells were seeded in 96-well plates at a density of 1×10^4 cells per well in 100 μL culture medium for 24 h. The culture medium was then removed and replaced with 100 μL new culture medium containing polysaccharides at a concentration of 0.125, 0.25, and 0.5 mg/mL for another 24 h. Subsequently, the polysaccharide was replaced by PBS and treated with 3 mJ/cm^2 UVB irradiation according to our previous study [12, 26]. Cell viability was measured according to the method in the cytotoxicity of PSF and isolated fractions.

The contents of MMP-1, MMP-3 and HYP in HaCaT cells

HaCaT cells were seeded at a density of 2×10^4 cells per well for 24 h. Subsequently, cells were cultured with polysaccharides dissolved in the medium, while the control and model groups were cultured in the medium for 24 h. HA (125 μg/mL) was added as a positive control. Thereafter, the cells were washed with PBS and then exposed to UVB (3 mJ/cm^2) by UVB illuminator. The control group was covered with tin foil to avoid UVB irradiation. The contents of MMP-1, MMP-3 and HYP in culture media

were analyzed using kits according to the manufacturer's instructions.

Methylation analysis

As described by Hu et al. [12], the type of glycosidic bonds was analyzed by methylation. Briefly, the P2 sample was dissolved in ultrapure water, and then N-Ethyl-N′-(3-dimethyl aminopropyl) carbodiimide hydrochloride (EDAC) was added to react for 2 h. Subsequently, imidazole and sodium boron deuteride were added sequentially for the reduction reaction for 3 h. The reaction was terminated by adding glacial acetic acid. The obtained product was reacted with methyl iodide (50 μL), extracted with dichloromethane, and dried with a nitrogen flow. After the sample was hydrolyzed with trifluoroacetic acid, reduced with ammonia and $NaBD_4$ or $NaBH_4$, and acetylated with acetic anhydride, the product was analyzed by a gas chromatograph-mass spectrometer (7890A-5977B, Agilent Technologies Inc., Santa Clara, CA, USA) equipped with a BPX70 capillary column (30 m × 0.25 mm × 0.25 μm, SGE, Australia) at 30–600 (*m*/*z*). The injector temperature was kept at 230 °C and helium was used as carrier gas. The initial temperature of the column oven was 140 °C for 2 min, and the temperature was increased to 230 °C at 3 °C/min for 3 min.

NMR determination

The sample P2 was dissolved in D_2O and analyzed by nuclear magnetic resonance spectroscopy (600 MHz AVANCE II, Bruker Technology Co., Ltd., Bergisch Gladbach, Germany). The nuclear magnetic resonance spectroscopy (NMR) spectra were performed at 25 ℃ and recorded the one-dimensional (including ^1H NMR and ^{13}C NMR) and two-dimensional (including COSY, HSQC and NOESY) nuclear magnetic resonance spectra.

Statistical analysis

All experiments were repeated in triplicate. The results were expressed as mean ± standard deviation. The significance of differences was assessed using a one-way analysis of variance (ANOVA) combined with Turkey's multiple comparison test by SPSS 22.0 software (SPSS Inc., Chicago, IL, USA).

Results and discussion

Physicochemical and structural characterization

Chemical composition

As shown in Fig. 1A, PSF was separated by DEAE Sepharose Fast Flow in the gradient elution of 0.2 M, 0.3 M and 0.4 M NaCl solutions to obtain three fractions in the 0.2 M, 0.3 M and 0.4 M NaCl, named P1, P2, and P3, with yields of 15.73, 13.99, and 4.71%, respectively. The chemical composition is summarized in Table 1. The contents of polyphenol and protein decreased to less than 1% after column isolation. The reducing sugar contents of all samples were less than 2% in total. In addition, the polysaccharide contents of PSF and three isolated polysaccharides were all higher than 70%, which could be deduced that the polysaccharide content of the three fractions (P1, P2, and P3) were relatively high. Moreover, the uronic acid contents of P1, P2 and P3 were 42.94 ± 3.42%, 40.75 ± 0.93%, and 2.21 ± 0.26%, respectively. Their sulfate contents were 3.01%, 10.05%, and 7.44%, respectively. Natural sulfated polysaccharides from marine animals and plants were assumed to be closely associated with biological activity [27]. The sum of the chemical compositions exceeds 100%, owing to cross-reactivity between the different substances in the color reaction.

The UV spectra of PSF and three isolated polysaccharides are shown in Fig. 1D. No absorption at 260 nm was observed in the UV scanning spectrum, indicating the absence of nucleic acid in PSF and isolated fractions. A weak absorption peak at 280 nm was observed for all the polysaccharides, suggesting that they might contain a small amount of protein, which was consistent with the results of the above chemical composition.

Molecular weight distribution

As exhibited in Fig. 1B, PSF and isolated fractions all exhibited relative symmetrical peaks, which indicated that they were polysaccharides with relative homogeneous molecular weight [28]. The average molecular weight information is listed in Table 1. P1 possessed the largest average molecular weight (208.89 kDa), which was similar to our previous study [12]. The average molecular weights of P2 and P3 were estimated to be 154.09 kDa and 151.71 kDa, respectively.

I_2-KI analysis

Sargassum fusiforme polysaccharides are mainly composed of fucoidan, alginate, laminarin, and dietary fiber [28]. Therefore, it is important to recognize whether the isolated polysaccharide contained starch. It is known that I_2 and I_3^- in KI-I_2 can react with branches and side chains in polysaccharides to form complexes, and the absorption peaks shift from 350 to 565 nm [29]. The UV–Vis spectrum of I_2-KI assays in Fig. 1C indicated that the PSF and isolated fractions did not contain starch.

Thermal analysis of polysaccharide

Differential scanning calorimetry (DSC) was used to measure the thermal stability of polysaccharides. As shown in Fig. 1F, PSF and isolated polysaccharides had similar endothermic and exothermic peaks in DSC

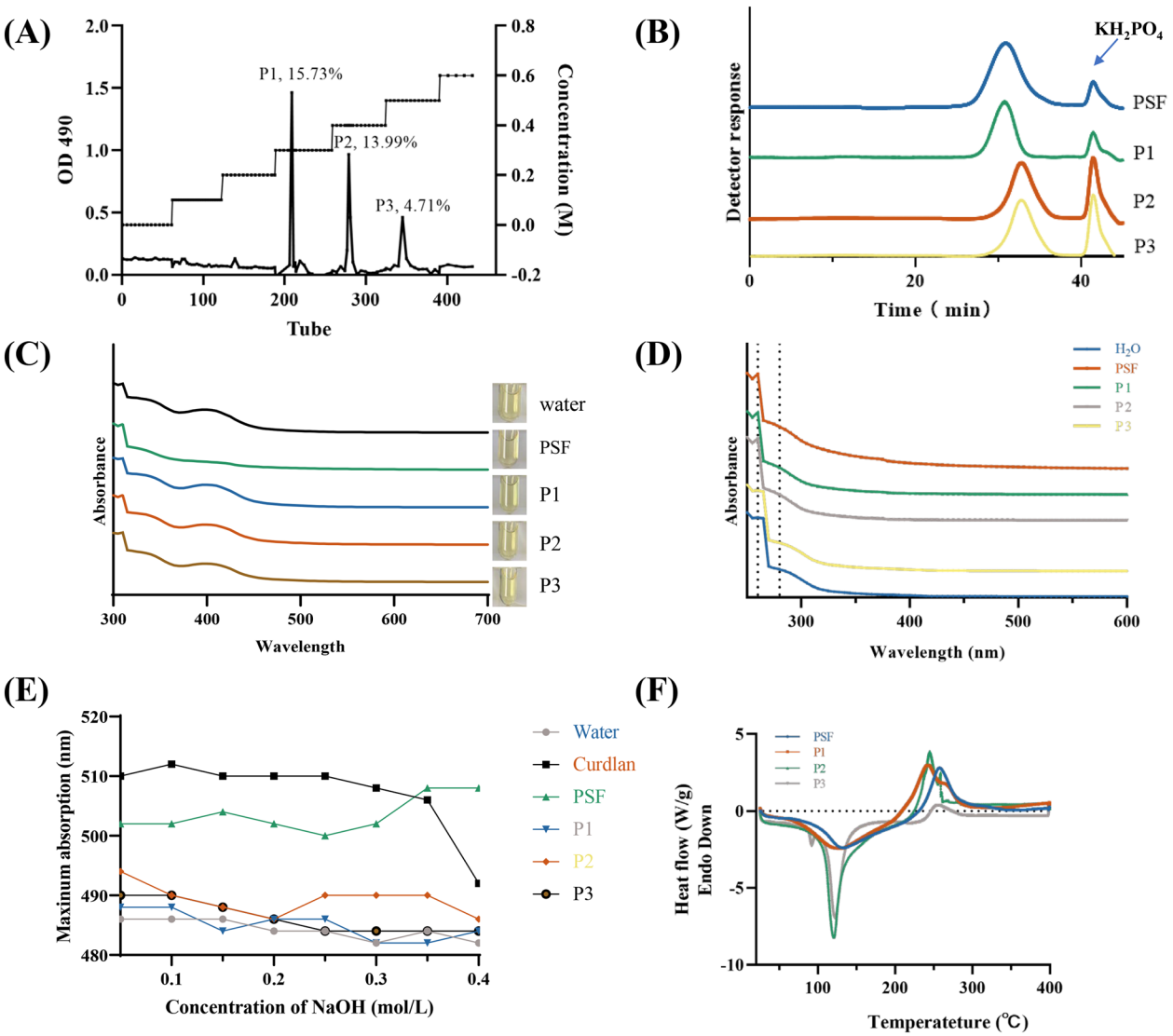

Fig. 1 The physicochemical properties of polysaccharides. **A** Elution curve of PSF; **B** molecular weight distribution; **C** UV–vis spectrum of polysaccharides in the presence of I_2-KI; **D** UV–vis spectrum; **E** maximum absorption wavelengths of Congo red with polysaccharides mixtures at different NaOH concentrations; **F** thermal analysis by differential scanning calorimetry. Polysaccharides include PSF and isolated fractions (P1, P2 and P3)

curves. The first endothermic peaks of polysaccharide (80–200 ℃) were mainly caused by removing water or partial decomposition in the sample [30]. The weight loss onset at about 150 ℃ indicated that the polysaccharide was not easily degraded by heating. The second peak of exothermic peaks appeared in DSC curves (200–300 ℃), which was deduced that the redox reaction might happen [30]. The thermal behavior and the transition temperature were affected by the structure and functional groups of polysaccharides [24]. The results suggested that PSF and the three isolated fractions were likely to be structurally stable and have good thermal stability.

Helix–coil transition analysis

It is known that polysaccharides can exhibit a variety of different conformations in solution, such as single helix, double helix, triple helix, and aggregates [31]. The triple helical structure of polysaccharides plays an important role in their biological activities, such as antitumor and immunomodulatory activities [32]. Polysaccharides with

Table 1 Chemical composition analysis and average molecular weight

–	PSF	P1	P2	P3
Polysaccharide (%)	72.19 ± 2.44^{a}	74.94 ± 2.33^{a}	72.44 ± 1.19^{a}	76.25 ± 0.08^{a}
Polyphenol (%)	0.34 ± 0.02^{a}	0.06 ± 0.02^{b}	0.1 ± 0.02^{b}	0.1 ± 0.03^{b}
Protein (%)	2.15 ± 0.09^{a}	0.33 ± 0.03^{b}	0.14 ± 0.08^{b}	0.15 ± 0.04^{b}
Reducing sugar (%)	1.77 ± 0.14^{a}	1.22 ± 0.06^{b}	1.53 ± 0.01^{a}	1.52 ± 0.14^{a}
Sulfate (%)	5.17 ± 0.26^{c}	3.01 ± 0.18^{d}	10.05 ± 0.28^{a}	7.44 ± 0.05^{b}
Uronic acid (%)	21.3 ± 1.66^{b}	42.94 ± 3.42^{a}	40.75 ± 0.93^{a}	2.21 ± 0.26^{c}
Mw (kDa)	157.74	208.89	154.09	151.71

Different marks (a–d) in each row represent the significant difference ($p < 0.05$)

triple helix conformation bound to Congo red showed a red shift in λmax in dilute solution and a sharp decrease in λmax in concentrated alkaline solution [33]. As shown in Fig. 1E, λmax values of PSF and three isolated fractions were stable with increasing NaOH concentration, indicating that all tested polysaccharides did not have a triple-helix structure.

FT-IR analysis

The FT-IR spectra of PSF and the three isolated polysaccharides had similar absorption peaks (Fig. 2A). The broad intense peaks at around 3400 cm^{-1} represented the stretching vibrations of –OH [34]. The weak peak at 2900 cm^{-1} was due to the C–H stretching [12]. Absorbances at 1620 cm^{-1} and 1420 cm^{-1} were assigned to stretching vibrations of COO–, which indicated that they might contain uronic acid [35]. The peak at 1250 cm^{-1} showed the S=O stretching vibration, suggesting the presence of a sulfate group [30]. The bands at 890 cm^{-1} and 830 cm^{-1} contributed to β-type and α-type glycosidic linkages, respectively [36, 37]. It was observed that PSF and isolated fractions had similar FT-IR spectra, and no new peaks appeared, which indicated that the PSF and the isolated fractions all contained similar functional groups.

Monosaccharide composition

The monosaccharide compositions of PSF and the three fractions were shown in Fig. 2B, PSF mainly consisted of Fuc (18.16%), GlcA (6.99%), and ManA (48.67%). P1 and P2 were composed of almost the same monosaccharide but with different ratios. Both of them were mainly composed of ManA (84.02% and 78.69%, respectively), which was consistent with our previous study [11], followed by minor amounts of Gal, GalA, Glc, Xyl, Fuc, Ara, GlcA, GulA, and Man. P3 had a relatively high proportion in Fuc (20.96%), Gal (13.08%), Xyl (12.33%), Man (13.62%), GlcA (11.37%), and ManA (21.40%), followed by Rha, Ara, Glc, GalA, and GulA.

Scanning electron microscopic observation

The microstructures of PSF and the three isolated fractions were observed at 500 × and 2000 × (Fig. 3). Both PSF and P1 had a dense reticular layer with rough and pore structures, whereas P2 and P3 exhibited relatively flaky appearance strips with hole structure. The surface morphology might be affected by the method of extraction, purification, or preparation of the samples [10]. Polysaccharides with higher molecular weight tend to form hydrogen bonds between polysaccharides [38]. It could be deduced that column chromatography isolation could separate the polysaccharides, leading to a relatively

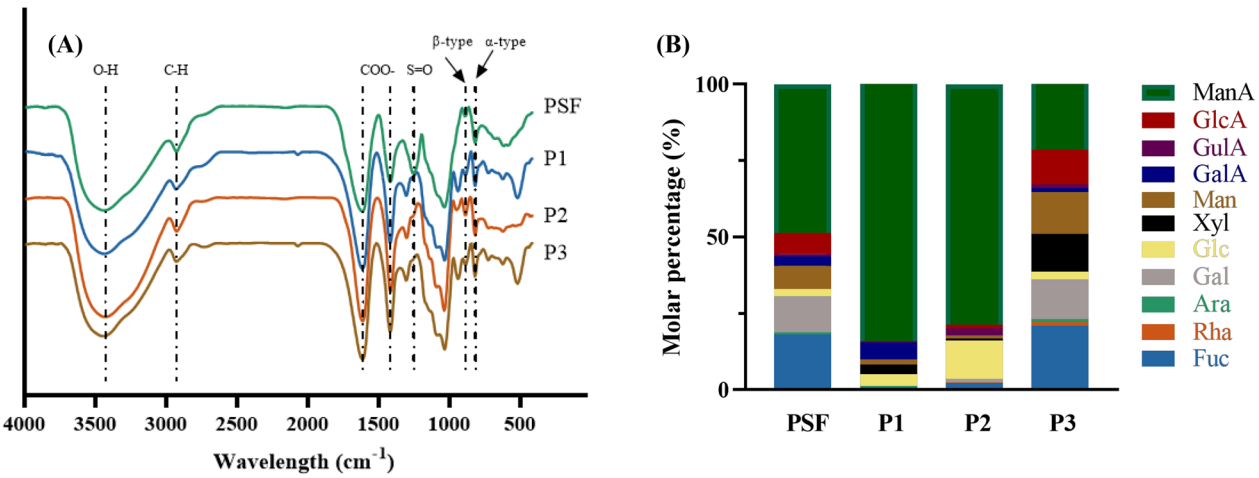

Fig. 2 **A** FT-IR spectra of PSF and isolated fractions (P1, P2 and P3); **B** Monosaccharide composition of PSF and isolated fractions (P1, P2 and P3)

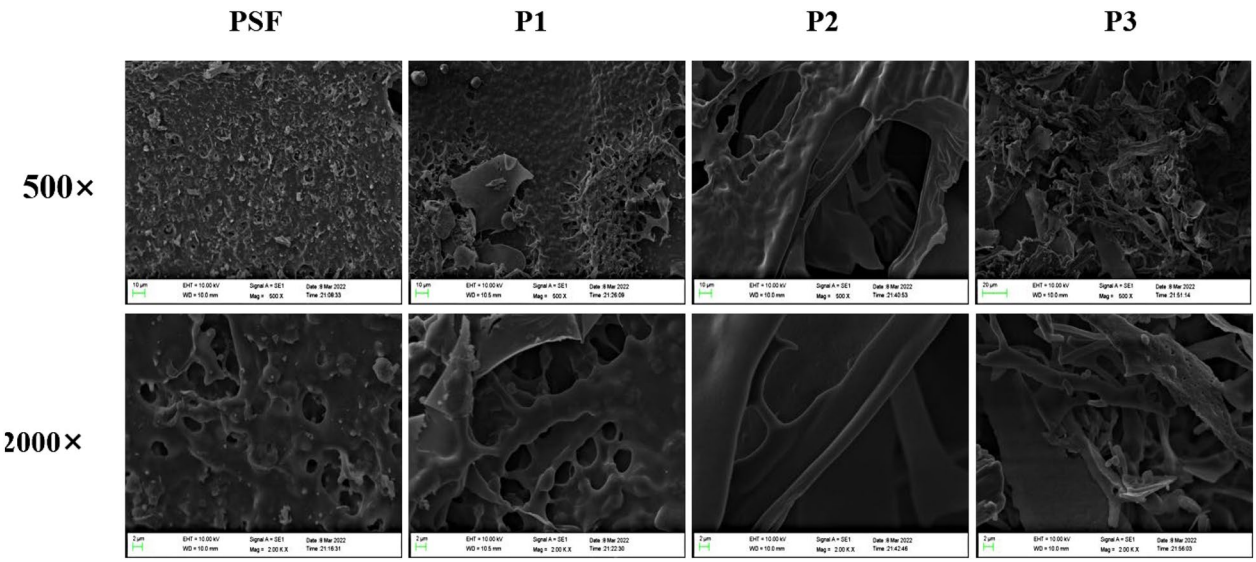

Fig. 3 SEM spectra of PSF and isolated fractions (P1, P2 and P3) at 500× and 2000×

loose microstructure in the isolated polysaccharide fractions.

Anti-photoaging activity in vitro

MTT assay was performed to examine the cytotoxic effect of polysaccharide on HaCaT cells (Fig. 4A). Cells were treated with various concentrations (0.1, 0.25, 0.5, and 1 mg/mL) and cultured for 12 h. HA and P3 showed cytotoxicity on HaCaT cells at a concentration of 1 mg/mL. Therefore, the concentrations of 0.1, 0.25 and 0.5 mg/mL were selected for the following study. UVB irradiation significantly decreased the viability of HaCaT cells to about 30% (Fig. 4B). In contrast, pretreating with HA could keep the cell viability level as the control group. Moreover, pretreatment with PSF and isolated polysaccharides (P1, P2 and P3) had higher cell viability compared with the model group. In particular, P2 showed the best ability among the three isolated fractions to prevent HaCaT cells from UVB damage.

Degradation of skin collagen and elastin caused by MMPs is a characteristic of prolonged exposure to solar ultraviolet and is thought to contribute to the appearance of wrinkles in sun-exposed skin [39]. UVB stimulation remarkably increased the secretion of MMP-1 and MMP-3 in HaCaT cells (Fig. 4C and D), whereas pretreating with HA could reduce the secretion of MMPs. PSF and three isolated polysaccharides could inhibit the secretions of MMP-1 and MMP-3. Among them, P2 possessed the strongest inhibition effect of MMPs in protecting HaCaT cells from UVB irradiation.

The content of HYP in the supernatant of HaCaT cells could reflect the metabolism of collagen, which indirectly reflected the synthesis and degradation of ECM [26]. As shown in Fig. 4E, PSF and isolated polysaccharides significantly increased the contents of HYP in HaCaT cells compared to the model group, but there was no significant difference among the polysaccharide groups. UVB damages the skin cells by inducing the overproduction of reactive oxygen species, disrupting cellular redox homeostasis, and triggering a complex signaling cascade that stimulates high expression of matrix metalloproteinases (MMPs), thereby degrading extracellular matrix compositions (ECM) and altering the composition of skin cells [40]. The loss of structural integrity of ECM is thought to contribute to wrinkle development and skin laxity [26]. The increased expression of MMPs is responsible for the destruction of ECM integrity in photoaged skin. As important members of matrix metalloproteinase (MMPs), MMP-1 and MMP-3 are responsible for the breakdown of type I procol-lagen, type IV collagen and other structural proteins in ECM [41].

The chemical structure of polysaccharides is vital for biological activity. Studies have shown that molecular weight, uronic acid and sulfate group content, monosaccharide type, and spatial conformation all affect the activity of polysaccharides [42, 43]. P2 had a moderate molecular weight and a higher sulfate content as compared to other fractions, which might be the reason for its higher anti-photoaging activity. In addition, P2 contained higher mannuronic acid, which has been reported to have potential immunotherapeutic, immunomodulatory and anti-inflammatory activities, revealing its possible contribution to biological activity [44].

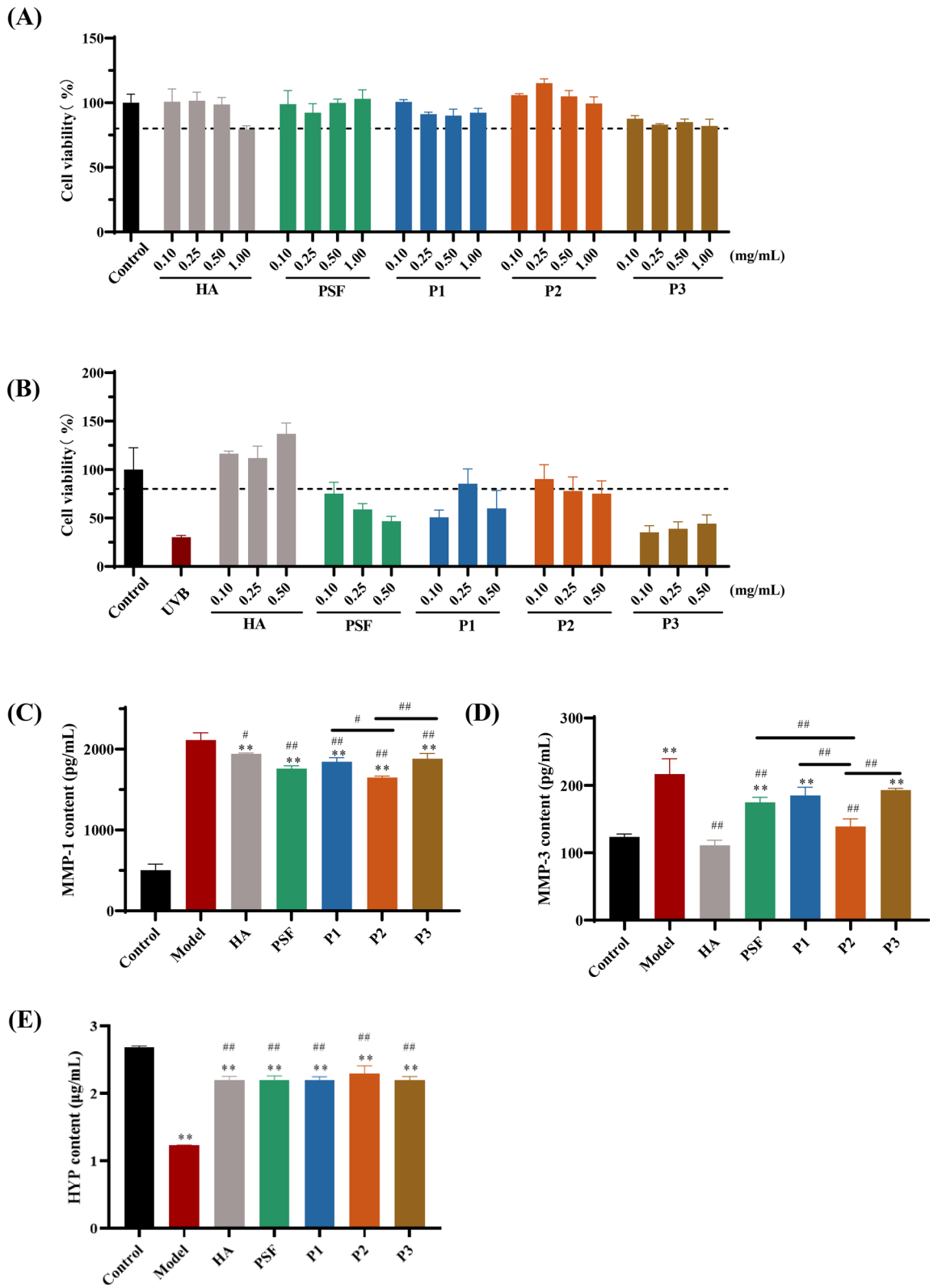

Fig. 4 UVB-induced photoaging in HaCaT cells and anti-photoaging activity of polysaccharides. **A** Effect of polysaccharides on cell viability; **B** effect of polysaccharides on cell viability of photoaged cells; **C** effect of polysaccharides on the level of MMP-1; **D** effect of polysaccharides on the level of MMP-3; **E** effect of polysaccharides on the level of HYP. Polysaccharides include PSF and isolated fractions (P1, P2 and P3). *$p < 0.05$ or **$p < 0.01$ vs. Control group; #$p < 0.05$ or ##$p < 0.01$

Methylation analysis

Based on the higher anti-photoaging activity, P2 was selected for further structural identification. Methylation analysis is a typical technique to elucidate the types of polysaccharides [45]. Therefore, P2 was methylated, hydrolyzed, reduced and acetylated, followed by GC–MS analysis to identify the glycosidic bond type. The linkage patterns of P2 were identified using a spectral database based on partially methylated alditol acetates standard dates in the Complex Carbohydrate Research Center (CCRC) spectral database (https://www.ccrc.uga.edu/specdb/ms/pmaa/pframe.htm), retention durations and related literature, which are shown in Table 2. Seven methylated sugar residues were found, the type of linkage namely t-Glc*p*, 1, 3-Glc*p*, 1, 4-Glc*p*, 1, 4, 6-Glc*p*, t-Man*p*, 1, 4-Man*p* and 1, 3, 4-Man*p*, with a molar ratio of 7.49: 4.33: 24.2: 5.04: 6.99: 33.55: 18.38. By comparing the major mass fragments of methylated polysaccharide after reduction by EDC-$NaBD_4$ and EDC-$NaBH_4$, and combining the results of the monosaccharide composition, t-Man*p*, 1, 4-Man*p* and 1, 3, 4-Man*p* might correspond to t-ManA, 1, 4-ManA and 1, 3, 4-ManA, respectively. The presence of 1, 4, 6-Glc*p* and 1, 3, 4-ManA indicated that P2 had a branched structure.

NMR analysis

The structure characteristic of P2 was further analyzed using NMR spectroscopy. 1D and 2D NMR spectra were used to analyze the detailed structure of P2. According to ^{13}C NMR (Fig. 5B), the peak at δ 177.53 ppm indicated the presence of uronic acid in P2, which was consistent with the results of monosaccharide composition analysis. The overlapping signals in NMR spectra were obtained, which could only provide limited information about the fine structure linkage. This was mainly attributed to the high viscosity, large molecular weight, and low solubility [21]. According to the ^{1}H and ^{13}C spectra (Fig. 5A and B), anomeric proton peaks δ 4.67, 4.64, 4.62, 4.57, 4.45, 4.41 and anomeric carbon signal peaks δ 103.69, 103.59, 103.58, 102.88, 101.34, 99.93, 99.92 suggested the existence of seven main glycosyl types. The signal at 5.05 ppm might be caused by α-L-guluronic acid H1 according to the studies [46, 47], which showed little content in the monosaccharide composition and methylation results. Consequently, we consider this peak to be the impurity component of the P2 fraction. In the ^{1}H-^{13}C HSQC spectrum (Fig. 5C), the cross-peaks were labeled as A (4.62/102.88 ppm), B (4.67/103.69 ppm), C (4.41/103.59 ppm), D (4.45/103.58 ppm), E (4.62/99.93 ppm), F (4.57/99.92 ppm) and G (4.64/101.34 ppm). In terms of residue A, the coupled peaks at δ H/H 4.62/3.48, 3.48/3.64, 3.64/3.7, 3.7/3.61, 3.61/3.89 (3.72) ppm were detected in ^{1}H-^{1}H COSY, so that the anomeric signals at δ 3.48, 3.64, 3.7, 3.61, 3.89 (3.72) ppm were assigned as H2–H6, respectively. Subsequently, according to the coupling peaks (δ H/C 3.48/72.48, 3.64/74.31, 3.7/68.99, 3.61/75.84 and 3.89/61.74) in HSQC, the signals at 72.48, 74.31, 68.99, 75.84 and 61.74 ppm were attributed to C2–C6, separately. Similarly, the chemical shift of residues B-G are labeled and listed in Table 3. The residues A–G were deduced based on literature reports and results of methylation analysis [12, 25, 47–49]. NOESY spectra were further used to deduce glycosidic linkages (Fig. 5E). The cross signal of δ 4.57/3.81 ppm (F H1/F H4) proved the linkage of →4)-β-D-ManA-(1→4)-β-D-ManA-(1→. In addition, the H-1 signal of residue F (δ 4.57 ppm) were correlated with H4 signal of residue G (δ3.68 ppm), illustrating the presence of →4)-β-D-ManA -(1→3, 4)-β-D-ManA-(1→. The cross peaks δ 4.64/3.66 ppm (G H1/B H3) revealed the linkage of →3, 4)-β-D-ManA-(1→3)-β-D-Glc*p*-(1→. The signal peak at δ 4.67/3.63 ppm (B H1/C H4) confirmed that the linkage of →3)-β-D-Glc*p*-(1→4)-β-D-Glc*p*-(1→. The cross signal at δ 4.41/3.57 ppm (C H1/D H4) was for →4)-β-D-Glc*p*-(1→4, 6)-β-D-Glc*p*-(1→. And the signal at δ 4.62/4.11 ppm (E H1/G H3) demonstrated the linkage of β-D-ManA-(1→3, 4)-β-D-ManA-(1→. Besides, the cross peak at δ4.62/4.13 ppm (A H1/D H6) indicated the linkage of β-D-Glc*p*-(1→4, 6)-β-D-Glc*p*-(1→. In

Table 2 Methylation analysis of P2

Type of linkage	Methylated alditol acetate	Relative molar ratio (%)	Mass fragments (*m/z*)
t-Glc(*p*)	1, 5-di-*O*-acetyl-2, 3, 4, 6-tetra-O-methyl gulitol	7.49	60, 69, 85, 102, 118, 137, 145, 162, 179, 205, 239
1, 3-Glc(*p*)	1, 3, 5-tri-*O*-acetyl-2, 4, 6-tri-*O*-methyl gulitol	4.33	60, 69, 85, 101, 118, 129, 137, 161, 203, 234
1, 4-Man(*p*)	1, 4, 5-tri-*O*-acetyl-2, 3, 6-tri-*O*-methyl mannitol	33.55	60, 71, 87, 102, 118, 129, 142, 162, 173, 233
1, 4-Glc(*p*)	1, 4, 5-tri-*O*-acetyl-2, 3, 6-tri-*O*-methyl gulitol	24.2	60, 69, 87, 102, 118, 129, 162, 173, 189, 233
t-Man(*p*)	1, 5-di-*O*-acetyl-2, 3, 4, 6-tetra-***O***-methyl mannitol	6.99	60, 69, 87, 102, 118, 129, 162, 233
1, 4, 6-Glc(*p*)	1, 4, 5, 6-tetra-*O*-acetyl-2, 3-tri-***O***-methyl gulitol	5.04	60, 69, 85, 102, 118, 127, 137, 159, 178, 201, 261, 338
1, 3, 4-Man(*p*)	1, 3, 4, 5-tetra-*O*-acetyl-2, 6-di-***O***-methyl mannitol	18.38	69, 84, 98, 117, 137, 159, 171, 185, 227, 239, 255, 311, 338

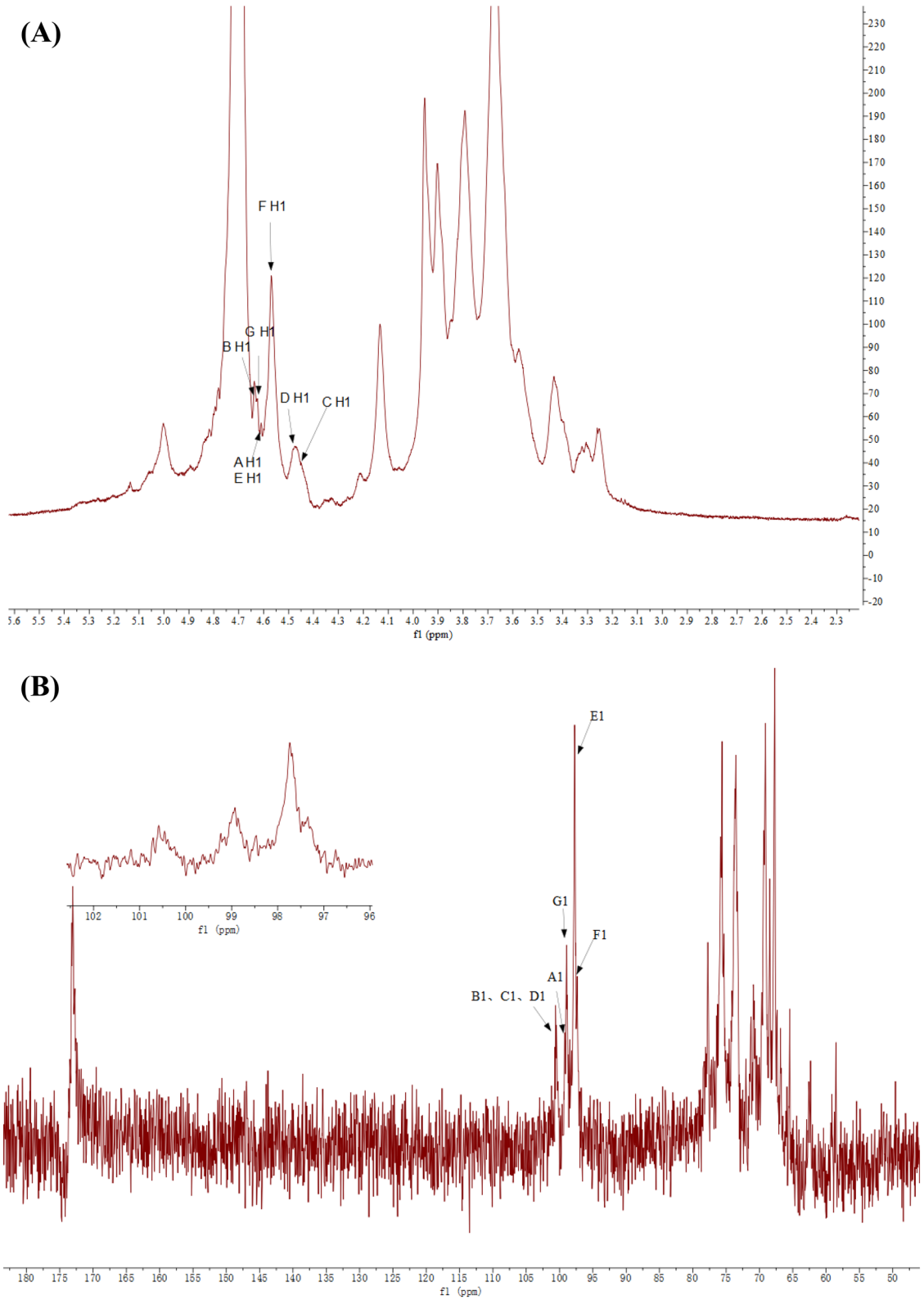

Fig. 5 NMR spectrum of P2 **A** 1H; **B** 13C; **C** HSQC; **D** COSY; **E** NOESY; **F** presumed structure

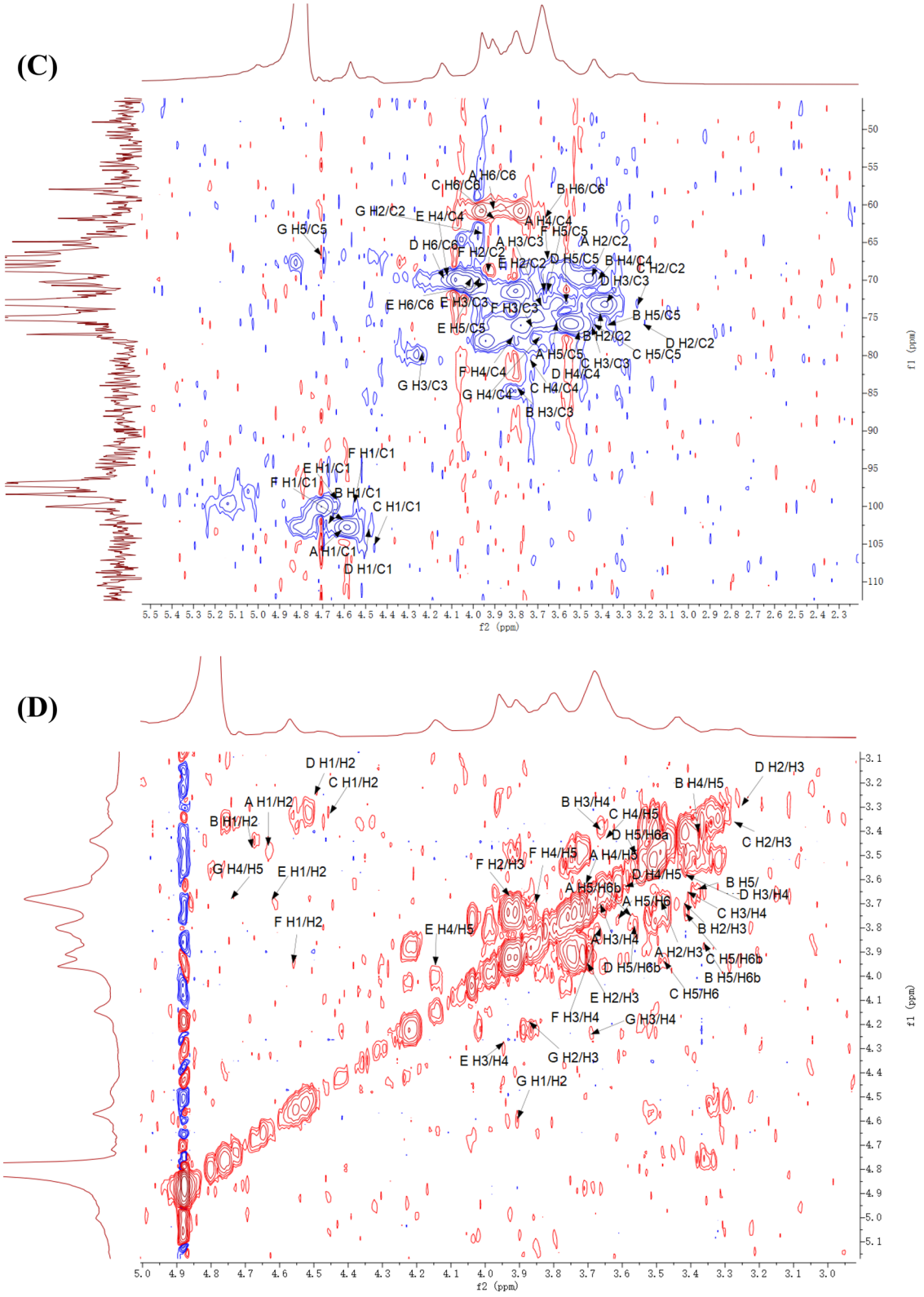

Fig. 5 continued

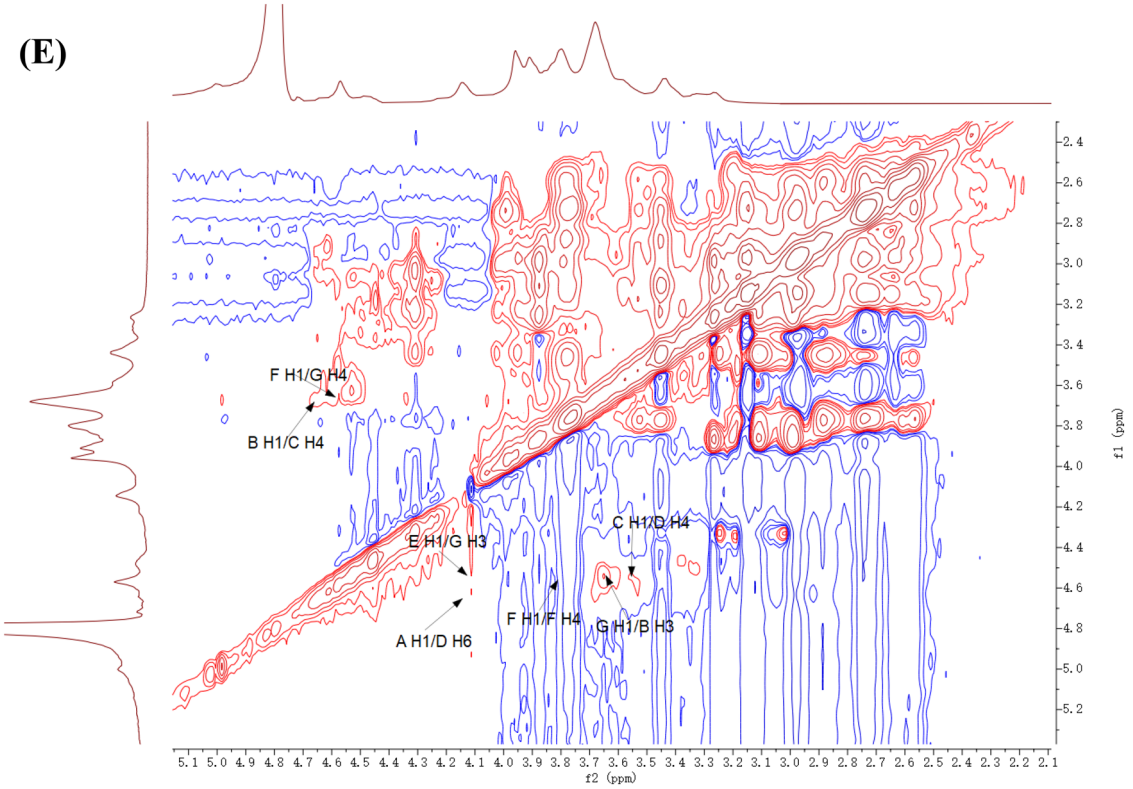

Fig. 5 continued

summary, we hypothesize that the possible structure of P2 backbone was → [4)-β-D-ManA-(1]$_{23}$ → 4)-β-D-ManA-(1 → 3)-β-D-Glc*p*-(1 → 4)-β-D-Glc*p*-(1 → 4)-β-D-Glc*p*-(1 → , and the end groups β-D-ManA-(1 → and β-D-Glc*p*-(1 → were connected by the → 3, 4)-*O*-3 bond of β-D-ManA-(1 → and *O*-6 of → 4, 6)-β-D-Glc*p*-(1 → , respectively (Fig. 5F).

Conclusions

Three polysaccharide fractions (P1, P2, and P3) were obtained by hot aqueous extraction of *Sargassum fusiforme*, followed by column chromatography purification. And their structure and physicochemical characterizations were elucidated by chemical composition, molecular weight, FT-IR, monosaccharide composition, Helix–coil transition analysis, SEM and DSC analysis. Among them, P2 showed the strongest ability to increase cell viability and inhibit the secretions of MMP-1 and MMP-3 in

Table 3 Chemical shift assignments for P2

	Type of linkage	H1/C1	H2/C2	H3/C3	H4/C4	H5/C5	H6a/C6	H6b
A	β-D-Glc*p*-(1 →	4.62	3.48	3.64	3.7	3.61	3.89	3.72
		102.88	72.48	74.31	68.99	75.84	61.74	
B	→ 3)-β-D-Glc*p*-(1 →	4.67	3.44	3.66	3.38	3.39	3.62	3.8
		103.69	74.52	85.4	69.39	76.79	61.8	
C	→ 4)-β-D-Glc*p*-(1 →	4.41	3.25	3.39	3.63	3.42	3.9	3.74
		103.59	73.92	76.47	79.91	76.44	61.42	
D	→ 4, 6)-β-D-Glc*p*-(1 →	4.45	3.22	3.39	3.57	3.59	4.13	3.75
		103.58	76.45	73.85	77	75.16	69.95	
E	β-D-ManA-(1 →	4.62	3.69	3.96	4.12	3.91		
		99.93	71.11	69.089	69.02	70.31	175.22	
F	→ 4)-β-D-ManA-(1 →	4.57	3.95	3.69	3.81	3.68		
		99.92	69.87	75.55	77.76	71.34	174.99	
G	→ 3, 4)-β-D-ManA-(1 →	4.64	3.89	4.11	3.68	4.72		
		101.34	64.61	79.94	77.68	67.16	175.22	

HaCaT cells, which could be attributed to its high uronic acid and sulfate group content. Furthermore, the monosaccharide residues and linkage type of P2 were analyzed according to the methylation, GC–MS analysis and NMR spectrum. This study has provided some insights into the structural information of *Sargassum fusiforme* polysaccharides, and in particular, P2 has greater potential than P1 and P3 to be developed as a natural anti-photoaging ingredient. The following work will focus on the structure–activity relationship of P2 against skin photoaging.

Acknowledgements
Not applicable.

Author contributions
Shiyuan Chang: methodology, data curation, writing-original draft preparation. Chen Yifan: provided technical support. Huamai Qiu: revision, suggestion. Biyang Zhu: review and editing. Peter Chi Keung Cheung: review and editing. Lijun You: supervision and revision.

Funding
The work was funded by National Natural Science Foundation of China (22278153, 31972011 and 3211101620), Excellent Youth Foundation of Guangdong Scientific Committee (2021B1515020037), Guangdong Basic and Applied Basic Research Foundation (2023B1515040014), and the 111 Project (B17018), and the Theme Based Research Scheme of the Research Grants Council (RGC) of the Hong Kong Special Administrative Region (Project No. T21-604/19-R).

Availability of data and materials
The datasets used and/or analyzed during the current study are available from the corresponding author on reasonable request.

Declarations

Ethics approval and consent to participate
Not applicable.

Competing interests
There are no conflicts of interest or competing interests.

Author details
[1]School of Food Science and Engineering, South China University of Technology, 381 Wushan Road, Guangzhou 510640, Guangdong, People's Republic of China. [2]Research Institute for Food Nutrition and Human Health (111 Center), Guangzhou 510640, Guangdong, People's Republic of China. [3]Food & Nutritional Sciences Program, School of Life Sciences, Chinese University of Hong Kong, Hong Kong, People's Republic of China.

Received: 4 February 2024 Accepted: 20 April 2024
Published online: 06 May 2024

References

1. Polat S, Trif M, Rusu A, Šimat V, Čagalj M, Alak G, et al. Recent advances in industrial applications of seaweeds. Crit Rev Food Sci Nutr. 2023;63(21):4979–5008.
2. Santhoshkumar P, Yoha K, Moses J. Drying of seaweed: approaches, challenges and research needs. Trends Food Sci Technol. 2023;138:153–63.
3. Market data forecast Seaweed cultivation market size, growth. Share|2023–2028. 2022. https://www.marketdataforecast.com/market-reports/seaweed-cultivation-market. Accessed 27 Feb 2023.
4. Zheng L, Chen X, Cheong K. Current trends in marine algae polysaccharides: the digestive tract, microbial catabolism, and prebiotic potential. Int J Biol Macromol. 2020;151:344–54.
5. Yao W, Yong J, Lv B, Guo S, You L, Cheung P, Kulikouskaya V. Enhanced in vitro anti-photoaging effect of degraded seaweed polysaccharides by UV/H_2O_2 treatment. Mar Drugs. 2023;21:430.
6. Qiu S, Veeraperumal S, Tan K, et al. The in vitro anti-inflammatory mechanism of Porphyra haitanensis oligosaccharides on lipopolysaccharide-induced injury in IEC-6 cells. J Funct Foods. 2024;112:106005.
7. Zhang R, Zhang X, Tang Y, Mao J. Composition, isolation, purification and biological activities of *Sargassum fusiforme* polysaccharides: a review. Carbohyd Polym. 2020;228:115381.
8. Tian H, Liu H, Song W, Zhu L, Zhang T, Li R, et al. Structure, antioxidant and immunostimulatory activities of the polysaccharides from *Sargassum carpophyllum*. Algal Res. 2020;49:101853.

9. Chen H, Zhang L, Long X, Li P, Chen S, Kuang W, et al. *Sargassum fusiforme* polysaccharides inhibit VEGF-A-related angiogenesis and proliferation of lung cancer in vitro and in vivo. Biomed Pharmacother. 2017;85:22–7.
10. Chen X, You L, Ma Y, Zhao Z, Kulikouskaya V. Influence of UV/H2O2 treatment on polysaccharides from *Sargassum fusiforme*: physicochemical properties and RAW 264.7 cells responses. Food Chem Toxical. 2021;153:112246.
11. Wang L, Cui Y, Wang K, Fu X, Xu J, Gao X, et al. Anti-inflammatory effect of fucoidan isolated from fermented *Sargassum fusiforme* in *in vitro* and *in vivo* models. Int J Biol Macromol. 2022;222:2065–71.
12. Hu J, Yao W, Chang S, You L, Zhao M, Cheung P, et al. Structural characterization and anti-photoaging activity of a polysaccharide from *Sargassum fusiforme*. Food Res Int. 2022;157:111267.
13. Ji X, Guo J, Tian J, et al. Research progress on degradation methods and product properties of plant polysaccharides. J Light Ind. 2023;38(3):55–62.
14. Ji D, You L, Ren Y, Wen L, Zheng G, Li C. Protective effect of polysaccharides from *Sargassum fusiforme* against UVB-induced oxidative stress in HaCaT human keratinocytes. J Funct Foods. 2017;36:332–40.
15. Chen Y, Wang T, Zhang X, Zhang F, Linhardt R. Structural and immunological studies on the polysaccharide from spores of a medicinal entomogenous fungus Paecilomyces cicadae. Carbohydr Polym. 2021;254:117462.
16. Dubois M, Gilles K, Hamilton J, Rebers P, Smith F. Colorimetric method for determination of sugars and related substances. Anal Chem. 1956;28:350–6.
17. Li X, Xie Q, Huang S, Shao P, You L, Pedisić S. Digestion & fermentation characteristics of sulfated polysaccharides from *Gracilaria chouae* using two extraction methods in vitro and in vivo. Food Res Int. 2021;145:110406.
18. Bradford M. A rapid and sensitive method for the quantitation of microgram quantities of protein utilizing the principle of protein-dye binding. Anal Biochem. 1976;72:248–54.
19. Tang Y, Liu Y, He G, Cao Y, Bi M, Song M, et al. Comprehensive analysis of secondary metabolites in the extracts from different lily bulbs and their antioxidant ability. Antioxidants. 2021;10(10):1634.
20. Lindsay H. A colorimetric estimation of reducing sugars in potatoes with 3, 5-dinitrosalicylic acid. Potato Res. 1973;16:176–9.
21. Zhang X, Bi C, Shi H, Li X. Structural studies of a mannoglucan from *Cremastra appendiculata* (Orchidaceae) by chemical and enzymatic methods. Carbohyd Polym. 2021;272:118524.
22. Wang Z, Xie J, Shen M, Nie S, Xie M. Sulfated modification, characterization and property of a water-insoluble polysaccharide from *Ganoderma atrum*. Int J Biol Macromol. 2015;79:248–55.
23. Blumenkrantz N, Asboe-Hansen G. New method for quantitative determination of uronic acids. Anal Biochem. 1973;54(2):484–9.
24. Suvakanta D, Narsimha MP, Pulak D, Joshabir C, Biswajit D. Optimization and characterization of purified polysaccharide from *Musa sapientum* L. as a pharmaceutical excipient. Food Chem. 2014;149:76–83.
25. Cheng Y, Xie Y, Ge J, Wang L, Peng D, Yu N, et al. Structural characterization and hepatoprotective activity of a galactoglucan from Poria cocos. Carbohyd Polym. 2021;263:117979.
26. Kang M, Yumnam S, Kim S. Oral intake of collagen peptide attenuates ultraviolet B irradiation-induced skin dehydration in vivo by regulating hyaluronic acid synthesis. Int J Mo Sci. 2018;19(11):3551.
27. Wang Z, Xie J, Shen M, Nie S, Xie M. Sulfated modification of polysaccharides: synthesis, characterization and bioactivities. Trends Food Sci Tech. 2018;74:147–57.
28. Wang Y, Guo M. Purification and structural characterization of polysaccharides isolated from *Auricularia cornea* var. Li. Carbohyd Polym. 2020;230:115680.
29. Chen X, Zhang R, Li Y, Li X, You L, Kulikouskaya V, et al. Degradation of polysaccharides from *Sargassum fusiforme* using UV/H_2O_2 and its effects on structural characteristics. Carbohyd Polym. 2020;230:115647.
30. Wang Y, Peng Y, Wei X, Yang Z, Xiao J, Jin Z. Sulfation of tea polysaccharides: synthesis, characterization and hypoglycemic activity. Int J Biol Macromol. 2010;46(2):270–4.
31. Ma C, Bai J, Shao C, Liu J, Zhang Y, Li X, et al. Degradation of blue honeysuckle polysaccharides, structural characteristics and antiglycation and hypoglycemic activities of degraded products. Food Res Int. 2021;143:110281.
32. Guo X, Kang J, Xu Z, Guo Q, Zhang L, Ning H, et al. Triple-helix polysaccharides: formation mechanisms and analytical methods. Carbohyd Polym. 2021;262:117962.
33. Guo R, Ai L, Cao N, Ma J, Wu Y, Wu J, et al. Physicochemical properties and structural characterization of a galactomannan from *Sophora alopecuroides* L. seeds. Carbohyd Polym. 2016;140:451–60.
34. Xie Q, Zheng X, Li L, Ma L, Zhao Q, Chang S, et al. Effect of curcumin addition on the properties of biodegradable pectin/chitosan films. Molecules. 2021;26(8):2152.
35. Liang J, Zhao Y, Yang F, Zheng L, Ma Y, Liu Q, et al. Preparation and structure-activity relationship of highly active black garlic polysaccharides. Int J Biol Macromol. 2022;220:601–12.
36. Chen J, Zhou M, Liu M, Bi J. Physicochemical, rheological properties and in vitro hypoglycemic activities of polysaccharide fractions from peach gum. Carbohyd Polym. 2022;296:119954.
37. Xue H, Xu J, Zhang J, Wei Y, Cai X, Tan J. Modeling, optimization, purification, and characterization of polysaccharides from *Lilium lancifolium Thunb*. LWT. 2022;162:113491.
38. Ji X, Guo J, Ding D, Gao J, Hao L, Guo X, et al. Structural characterization and antioxidant activity of a novel high-molecular-weight polysaccharide from *Ziziphus Jujuba* cv. *Muzao*. J Food Meas Charact. 2022;16:2191–200.
39. Fisher G, Datta S, Harvinder S, Wang Z, James V, Kang S, et al. Molecular basis of sun-induced premature skin ageing and retinoid antagonism. Nature. 1996;379:335–9.
40. Yao W, Chen X, Li X, Chang S, Zhao M, You L. Current trends in the anti-photoaging activities and mechanisms of dietary non-starch polysaccharides from natural resources. Crit Rev Food Sci. 2022;62(32):9021–35.
41. Jose A, Zena W. Matrix metalloproteinases and their expression in mammary gland. Cell Res. 1998;8:187–94.
42. Jin W, Zhang W, Liang H, Zhang Q. The structure-activity relationship between marine algae polysaccharides and anti-complement activity. Mar Drugs. 2016;14(1):3.
43. Wang B, Yan L, Guo S, Wen L, Yu M, Feng L, et al. Structural elucidation, modification, and structure-activity relationship of polysaccharides in chinese herbs: a review. Front Nutr. 2022;9:908175.
44. Li Q, Bai D, Qin L, Shao M, Zhang S, Yan C, et al. Protective effect of d-tetramannuronic acid tetrasodium salt on UVA-induced photo-aging in HaCaT cells. Biomed Pharmacother. 2020;126:110094.
45. Ji X, Yan Y, Hou C, et al. Structural characterization of a galacturonic acid-rich polysaccharide from *Ziziphus Jujuba* cv. *Muzao*. Int J Biol Macromol. 2020;147:844–52.
46. Grasdalen H. High-field, 1H-n.m.r. spectroscopy of alginate: sequential structure and linkage conformations. Carbohyd Res. 1983;118:255–60.
47. Cong Q, Xiao F, Liao W, Dong Q, Ding K. Structure and biological activities of an alginate from *Sargassum fusiforme*, and its sulfated derivative. Int J Biol Macromol. 2014;69:252–9.
48. Martínez-Gómez F, Mansilla A, Matsuhiro B, Matulewicz M, Troncoso-Valenzuela M. Chiroptical characterization of homopolymeric block fractions in alginates. Carbohyd Polym. 2016;146:90–101.
49. Matsuo K, Isogai E, Araki Y. Occurrence of [→3)-β-d-Manp-(1→4)-β-d-Manp-(1→]n units in the antigenic polysaccharides from *Leptospira biflexa* serovar patoc strain Patoc I. Carbohy Res. 2000;328(4):517–24.

Publisher's Note

Springer Nature remains neutral with regard to jurisdictional claims in published maps and institutional affiliations.